

Gravitational waves and black holes from the phase transition in models of dynamical symmetry breaking

Martín Arteaga,^a Anish Ghoshal,^b Alessandro Strumia.^c

^a*Facultad de Ingeniería y Arquitectura, Universidad Autónoma del Perú, Lima, Perú*

^b*Institute of Theoretical Physics, Faculty of Physics, University of Warsaw, Poland*

^c*Dipartimento di Fisica, Università di Pisa, Italia*

E-mail: martin.arteaga@autonoma.pe, anish.ghoshal@fuw.edu.pl,
alessandro.strumia@unipi.it

Abstract. Theories of dynamical electroweak symmetry breaking predict a strong first order cosmological phase transition: we compute the resulting signals, primordial black holes and gravitational waves. These theories employ one SM-neutral scalar, plus some extra model-dependent particle to get the desired quantum potential out of classical scale invariance. We consider models where the extra particle is a scalar singlet, or vectors of an extended U(1) or SU(2) gauge sector. In models where the extra particle is stable, it provides a particle Dark Matter candidate with freeze-out abundance that tends to dominate over primordial black holes. These can instead be DM in models without a particle DM candidate. Gravitational waves arise at a level observable in future searches, even in regions where DM cannot be directly tested.

Contents

1	Introduction	1
2	Formalism for dynamical electroweak symmetry breaking	2
2.1	Computing the thermal potential	3
2.2	Computing the phase transition	4
2.3	Gravitational waves from the phase transition	5
2.4	PBH formation from strong first-order phase transition	6
3	Minimal model with singlet scalar DM	7
3.1	Primordial Black Holes as DM	10
3.2	General parameter space of the model	11
3.3	Particles as DM	13
4	Model with SU(2) vector DM	13
5	Model with U(1)_{B-L} gauge group	15
6	Discussion and Conclusion	16

1 Introduction

The LIGO-VIRGO-KAGRA interferometers [1] and Pulsar Timing Arrays [2–5] confirmed the expected existence of gravitational waves (GW). The observed signals seem likely due to astrophysical sources. The observation of a Stochastic Background of GW (SGWB) produced during the Big Bang would have a fundamental significance. SGWB are a unique probe of the early Universe, as the Universe is transparent to GWs right from the wee moments of the Big Bang, unlike other cosmic relics like photons and neutrinos. Although LIGO-VIRGO only set an upper limit on SGWB [6–8], increased sensitivity in the nHz-kHz frequency range should be reached by possible future observations such as SKA [9], GAIA/THEIA [10], MAGIS [11], AION [12], AEDGE [13], μ ARES [14], LISA [15], TianQin [16], Taiji [17], DECIGO [18], BBO [19], ET [20], CE [21]. GW searches at MHz-GHz higher frequencies are discussed [22–25].

Among various cosmological mechanisms for producing a SGWB [26], cosmological strong first-order phase transitions (FOPTs) (see e.g. [27]) offer plausible beyond the Standard Model (BSM) signals, up to high scales. Indeed the SM predicts two (electroweak and QCD) phase transitions, none of which is of first-order [28, 29]. Therefore, the detection of a GW signal compatible with a FOPT would be evidence of BSM physics. FOPTs develop by the formation of bubbles that expand, collide and percolate. The violent collisions between the bubble walls (and the motion of the surrounding thermal plasma) lead to the production of stochastic GWs. The typical frequency of such gravitational waves is the red-shifted Hubble rate during the phase transition, $f_{\text{peak}} \sim T_0 T / M_{\text{Pl}}$. A FOPT around the electroweak scale, $T \sim 100$ GeV, would peak at $f \sim$ mHz [30] which is in the frequency sensitivity band of space-based GW experiments such as LISA [15], whereas ground-based experiments such as

LIGO-VIRGO [31, 32] and ET [20] around 100 Hz can probe FOPTs up to $T \sim 10^8$ GeV [33], beyond the reach of collider experiments.

A detectable GW signal arises if the phase transition is strongly first-order. This is fulfilled by approximately scale-invariant theories [34], where scale symmetry is broken dynamically through the Coleman-Weinberg mechanism [35] after a significant amount of supercooling [36]. So, bubble collisions take place in the vacuum, enhancing the amplitude of the corresponding GW signal [37–39].¹

In this work we analyze the cosmological implications of such BSM phase transitions. Besides an enhanced GW signal, a supercooled FOPT also leads to the formation of primordial black holes (PBHs) via different mechanisms. Bubble collisions have been studied e.g. in [58]. We focus on a mechanism suggested in [59–64] that recently received interest [65–87]. FOPTs proceed via the nucleation of bubbles of the broken phase in an initial background of the symmetric phase [88–90]. In a supercooled regime, the energy density of the Universe in the symmetric phase is dominated by the vacuum energy which acts as a cosmological constant and leads to an inflationary period. In a nucleated bubble, instead, such energy is quickly converted into radiation and the corresponding patch expands slower. Since bubble nucleation is a stochastic phenomenon, and since, in a supercooled regime, regions outside the nucleated bubbles dilute faster than those inside, a region where nucleation happens later becomes over-dense and eventually collapses, if large enough, into a PBH.

The paper is organised as follows. In section 2 we present the basic framework and summarise standard results about how gravitational waves and Primordial Black Holes are later computed in specific models:

- In section 3 we consider a minimal model that realises dynamical electroweak symmetry breaking by adding two scalars to the SM: a singlet s that acquires a vacuum expectation value, and another singlet s' (a possible DM candidate) with couplings that induce the needed quantum effects.
- In section 4 we consider a model where s is doublet under an extra $SU(2)$ group; its vectors are stable and provide DM candidates.
- In section 5 we consider a model where s is charged under a $U(1)$ gauge group, that we identify as $U(1)_{B-L}$ such that there is no particle DM. Only Primordial Black Holes provide viable Dark Matter candidates.

These different models provide similar signals. Conclusions and a summary of results are given in section 6.

2 Formalism for dynamical electroweak symmetry breaking

Dimension-less scalar potentials with quartic couplings that run to negative values when renormalized down to low energy lead to dynamical symmetry breaking [35] via a first-order phase transition. This mechanism can induce the breaking of the electroweak symmetry. The minimal implementation with just the Standard Model Higgs doublet H is excluded because it predicts a too light Higgs boson, $m_h \approx 7$ GeV [91]. This wrong prediction is avoided by

¹See e.g. [40–52] for explorations of this mechanism in other BSM contexts. This has also been used in the context of baryogenesis via leptogenesis [53–55], complementarity with collider searches [56] and of the generation of the Planck scale [57].

adding an extra scalar s neutral under the SM gauge group. The tree-level scalar potentials have the form

$$V_{\text{tree}}(H, s) = V_\Lambda + \lambda_H |H|^4 + \frac{\lambda_S}{4} s^4 + \frac{\lambda_{HS}}{2} |H|^2 s^2 + \dots \quad (2.1)$$

where \dots denotes possible extra scalars. If the beta function of λ_S is positive, $\beta_{\lambda_S} = d\lambda_S/d\ln\mu > 0$, the loop potential

$$V_{\text{loop}}(0, s) \simeq \lambda_S(s) \frac{s^4}{4} \simeq \frac{\beta_{\lambda_S}}{2} \frac{s^4}{4} \ln \frac{s^2}{w^2 e^{1/2}} \quad (2.2)$$

has a minimum at $\langle s \rangle = w$, where w effectively is a free parameter. The s mass is loop suppressed, $m_s = w\sqrt{\beta_{\lambda_S}}$. The dimensionful constant $V_\Lambda \approx \beta_{\lambda_S} w^4/16$ needs to be added to eq. (2.1) such that the loop potential vanishes at its minimum, as required by the tiny observed cosmological constant. A small negative value of $\lambda_{HS} < 0$ then leads to electroweak dynamical symmetry breaking as

$$H = \frac{1}{\sqrt{2}} \begin{pmatrix} 0 \\ h \end{pmatrix}, \quad \langle h \rangle = v \simeq w \sqrt{\frac{-\lambda_{HS}}{2\lambda_H}} \quad (2.3)$$

in the unitary gauge. Here $\lambda_H \approx 0.126$ is the SM Higgs quartic, up to small corrections. During the Big Bang, s acquires a thermal mass such that the universe initially remains trapped in the false vacuum at $s = h = 0$. This super-cooling starts at the temperature T_{eq} such that the potential energy becomes more important than the thermal energy

$$\frac{\pi^2 g_* T_{\text{eq}}^4}{30} = V_\Lambda \quad (2.4)$$

with $g_* \approx 106.75$ the number of SM degrees of freedom. Next the temperature and thereby the thermal mass drops, and super-cooling can end via a first order phase transition that happens when nucleation becomes faster than the expansion rate. At this point the energy V_Λ stored in the potential gets released. We will focus on large enough couplings such that reheating is fast, so that the universe reheats up to temperature

$$T_{\text{RH}} \simeq T_{\text{eq}} \simeq w \left(\frac{15\beta_{\lambda_S}}{8\pi^2 g_*} \right)^{1/4}. \quad (2.5)$$

Extra particles are needed to get the desired $\beta_{\lambda_S} > 0$ running of λ_S , leading to a variety of models of dynamical electroweak symmetry breaking. Three models will be described and computed in sections 3, 4, 5. In this section we describe the model-independent common formalisms.

2.1 Computing the thermal potential

At finite temperature T , the potential of generic scalars ϕ receives an additive thermal contribution V_T given at leading order by the standard expression

$$V_T(\phi, T) = \frac{T^4}{2\pi^2} \sum_{\text{b}} J_B \left(\frac{m_{\text{b}}^2(\phi)}{T^2} \right) + \frac{T^4}{2\pi^2} \sum_{\text{f}} J_F \left(\frac{m_{\text{f}}^2(\phi)}{T^2} \right) \quad (2.6)$$

where ‘b’ and ‘f’ stand for all bosons and fermions present in the theory. The sums run over all field-dependent masses $m_{\text{b,f}}^2(\phi)$. The thermal integrals J_B and J_F are

$$J_{B/F}(y^2) = \int_0^\infty dx x^2 \ln \left[1 \mp \exp \left(-\sqrt{x^2 + y^2} \right) \right]. \quad (2.7)$$

These functions have the small-field expansion

$$\begin{aligned} J_B(y^2) &\simeq -\frac{\pi^4}{45} + \frac{\pi^2}{12}y^2 - \frac{\pi}{6}y^3 + \frac{y^4}{32}\ln\frac{y^2}{a_B} + \dots, \\ J_F(x^2) &\simeq \frac{7\pi^4}{360} - \frac{\pi^2}{24}y^2 - \frac{y^4}{32}\ln\frac{y^2}{a_F} + \dots \end{aligned} \quad (2.8)$$

with $a_B = (4\pi)^2 e^{3/2-2-\gamma_E} = 16a_F$. The quadratic term dominates at small field values, so that positive squared thermal masses trap scalars at the local minimum $\langle s \rangle = \langle h \rangle = 0$ of V_T . For example, the SM contribution to the Higgs thermal mass is

$$M_{hT}^2 = \left(\frac{3}{16}g_2^2 + \frac{1}{16}g_Y^2 + \frac{1}{4}y_t^2 + \frac{1}{2}\lambda_H \right) T^2. \quad (2.9)$$

The thermal mass of s arises from its model-dependent couplings needed to have the running $\lambda_{\beta_S} > 0$. The quartic terms in $J_{B,F}$ imply that the quartic couplings get renormalised around T . The bosonic function J_B also contains to a cubic term, relevant in tunnelling computations.

2.2 Computing the phase transition

Following the standard tunnelling formalism, the space-time density of bubble nucleation rate at finite temperature is

$$\gamma \approx T^4 \left(\frac{S_3}{2\pi T} \right)^{3/2} e^{-S_3/T} \quad (2.10)$$

where S_3 is the action of the dominant O(3)-invariant thermal bounce. In our computations the tunnelling action S_3 is numerically computed from the thermal potential, that includes the full $J_{B,F}$ functions, plus higher-order ‘daisy’ contributions.

The following analytic approximation allows to understand the main features. The finite-temperature potential along the s direction can be approximated as

$$V \simeq \frac{m^2}{2}s^2 - \frac{k}{3}s^3 - \frac{\lambda}{4}s^4 + \dots \quad (2.11)$$

with roughly constant $\lambda = -\lambda_S(T) \simeq \beta_{\lambda_S} \ln(w/T) > 0$. This coupling runs larger at lower T , facilitating the phase transition. Indeed the bounce action corresponding to the potential of eq. (2.11) can be approximated as (see e.g. [83])

$$S_3 \approx \frac{27\pi m^3}{2k^2} \frac{1 + e^{-\tilde{\lambda}^{-1/2}}}{1 + 9\tilde{\lambda}/2}, \quad \tilde{\lambda} = \lambda \frac{m^2}{k^2}. \quad (2.12)$$

In the limit of negligible cubic coupling, $k = 0$, the action reduces to $S_3 \simeq 6\pi m/\lambda$. After crossing $\lambda = 0$, the running coupling λ becomes larger at lower temperature. So S_3/T tends to increase at lower T proportionally to $1/\ln(w/T)$. Super-cooling is ended by nucleation at low enough T_{nuc} provided that large enough couplings make tunnelling faster than the Hubble rate. The nucleation temperature T_{nuc} is defined as

$$\gamma(T_{\text{nuc}}) \approx H^4(T_{\text{nuc}}). \quad (2.13)$$

The Hubble rate is approximated as

$$H^2 = \frac{\rho_{\text{rad}} + V_\Lambda}{3M_{\text{Pl}}^2}, \quad \rho_{\text{rad}} = \frac{\pi^2}{30}g_*T^4 \quad (2.14)$$

with $\rho_{\text{rad}} \ll V_\Lambda$ during super-cooling. As a consequence the relative amount of released energy in a super-cooled phase transition is large $\alpha \approx V_\Lambda/\rho_{\text{rad}} \gg 1$, giving large gravitational wave signals.² The inverse duration of the phase transition is approximated as $\beta = d \ln \gamma / dt$ evaluated at the nucleation time t_{nuc} . It is convenient to introduce the dimensionless ratio [93]

$$\frac{\beta}{H} = - \left. \frac{d \ln \gamma}{d \ln T} \right|_{T=T_{\text{nuc}}} \simeq -4 + \frac{d}{d \ln T} \left(\frac{S_3}{T} - \frac{3}{2} \ln \frac{S_3}{T} \right) \Big|_{T=T_{\text{nuc}}} \quad (2.16)$$

so that the phase transition happens in H/β Hubble times. The duration of the phase transition gets longer, up to a fraction of Hubble time, in the regime where T_{nuc} is much smaller than the mass scales of the problem. This happens because $d(S_3/T)/d \ln T \propto \ln^{-2}(w/T)$ decreases at $T \ll w$, where the approximation of eq. (2.11) gets more accurate. As discussed later in section 2.4, a substantial amount of primordial black holes forms in this regime, near to the critical boundary where nucleation becomes too slow for ending super-cooling. If T gets smaller than Λ_{QCD} , super-cooling is ended by QCD effects [36, 43].

The probability that a point still is in the false vacuum phase at time t is $\wp(t) = e^{-I(t)}$, where (see e.g. [79, 80, 82])

$$I(t) = \frac{4\pi}{3} \int_{t_c}^t dt' \gamma(t') a^3(t') r^3(t, t') = \frac{4\pi}{3} \int_T^{T_c} \frac{dT' \gamma(T')}{T'^4 H(T')} \left(\int_T^{T'} \frac{d\tilde{T}}{H(\tilde{T})} \right)^3. \quad (2.17)$$

where nucleation starts at $t_c \lesssim t_{\text{eq}}$ and $r(t'', t') = \int_{t'}^{t''} dt v_{\text{wall}}/a$ is the radius at time t'' of a bubble formed at time t' . The percolation temperature T_{perc} is approximatively defined as $I(T_{\text{perc}}) = 0.34$ meaning that 34% of the comoving volume has been converted into the true minimum [50, 94, 95]. While in most of the parameter space $T_{\text{perc}} \approx T_{\text{nuc}}$, Primordial Black Hole formation will occur when the phase transition has a long duration $\beta/H \lesssim 8$, such that $T_{\text{perc}} \lesssim T_{\text{nuc}}$. The phase transition completes provided that the comoving volume $\mathcal{V}_{\text{false}} \propto a(t)^3 \wp(t)$ remaining in the false vacuum decreases [50, 94]

$$\left. \frac{d\mathcal{V}_{\text{false}}}{dt} \right|_{t \sim t_{\text{perc}}} < 0 \quad \text{i.e.} \quad 3 + \left. \frac{dI(T)}{d \ln T} \right|_{T \sim T_{\text{perc}}} < 0. \quad (2.18)$$

2.3 Gravitational waves from the phase transition

The gravitational wave spectrum generated from first-order phase transitions is dominated by three contributions: the collision of true vacuum bubbles, $\Omega_{\text{col}} h^2$; the propagation of sound waves within the plasma, $\Omega_{\text{sw}} h^2$; and magnetohydrodynamic turbulence effects, $\Omega_{\text{turb}} h^2$, as discussed in [96]. Bubble collisions dominate in our scenario, as supercooling leads to a large energy release $\alpha \gg 1$. The resulting $\Omega_{\text{col}} h^2$ is approximated as [92, 93, 97–101]

$$\Omega_{\text{col}} h^2 = 1.67 \cdot 10^{-5} \left(\frac{\beta}{H} \right)^{-2} \left(\frac{\kappa_{\text{col}} \alpha}{1 + \alpha} \right)^2 \left(\frac{100}{g_\star} \right)^{1/3} \Delta_{\text{col}}(v_{\text{wall}}) S_{\text{col}}(f). \quad (2.19)$$

²The parameter α , quantifying the strength of the transition, varies in definition across the literature, with primary interpretations focusing on latent heat and the trace anomaly [92]. It is generally defined as either the ratio of the transition's latent heat to the radiation energy density in the plasma, ρ_{rad} , or via the stress-energy tensor's trace and ρ_{rad} . These conceptualisations converge in the formula [93]:

$$\alpha = \frac{1}{\rho_{\text{rad}}} \left(\Delta V - n \frac{\partial \Delta V}{\partial \ln T} \right) \Big|_{T=T_n}, \quad (2.15)$$

where $\Delta V = V_{\text{eff}}(\langle \phi \rangle_{\text{false}}, T) - V_{\text{eff}}(\langle \phi \rangle_{\text{true}}, T)$ represents the free energy density difference between the two phases, and n assumes values of 1 or 1/4, corresponding to the definitions based on latent heat and trace anomaly, respectively.

The gravitational wave energy density Ω_{col} achieves its maximal α -independent value at $\alpha \gg 1$. The coefficient κ_{col} is the efficiency associated to collisions of scalar shells (see e.g. [94]). In view of $\alpha \gg 1$, we assume $\kappa_{\text{col}} \approx 0.95$ [65]. The function of the wall velocity v_{wall} in eq. (2.19) is [50]

$$\Delta_{\text{col}}(v_{\text{wall}}) = \frac{0.48 v_{\text{wall}}^3}{1 + 5.3 v_{\text{wall}}^2 + 5 v_{\text{wall}}^4}. \quad (2.20)$$

meaning that larger v_{wall} leads to stronger GW signals. In view of $\alpha \gg 1$ we can assume highly relativistic bubbles, $v_{\text{wall}} \simeq 1$ [50, 65, 102]. The spectral shape $S_i(f)$ in eq. (2.19) is [98–101]

$$S_{\text{col}}(f) = \left[c_l \left(\frac{f}{f_{\text{col}}} \right)^{-3} + (1 - c_l - c_h) \left(\frac{f}{f_{\text{col}}} \right)^{-1} + c_h \left(\frac{f}{f_{\text{col}}} \right) \right]^{-1} \quad (2.21)$$

where $c_l = 0.064$ and $c_h = 0.48$. S_{col} equals unity at the peak frequency f_{col} given by

$$f_{\text{col}} = 1.65 \times 10^{-5} \text{ Hz} \Xi_{\text{col}}(v_{\text{wall}}) \frac{\beta}{H} \frac{T_{\text{RH}}}{100 \text{ GeV}} \left(\frac{g_{\star}}{100} \right)^{1/6} \quad \text{for} \quad T_{\text{RH}} \gg T_{\text{nuc}} \quad (2.22)$$

with [92, 93, 97]

$$\Xi_{\text{col}}(v_{\text{wall}}) = \frac{0.35}{1 + 0.069 v_{\text{wall}} + 0.69 v_{\text{wall}}^4}. \quad (2.23)$$

Big Bang Nucleosynthesis (BBN) and Cosmic Microwave background (CMB) data provide a bound on the energy density of extra radiation (in this case, of gravitational waves). Such bound is usually presented in terms of an effective number of extra neutrinos [103]

$$\Delta N_{\text{eff}} = 4.4 \left. \frac{\rho_{\text{GW}}}{\rho_{\gamma}} \right|_0 = 1.8 \cdot 10^5 \int_{f_{\text{min}}}^{\infty} \frac{df}{f} \Omega_{\text{GW}}(f) h^2 \approx 10^5 \Omega_{\text{GW}}^{\text{peak}} h^2 \quad (2.24)$$

where we can approximate $f_{\text{min}} \approx 0$. The current bound $\Delta N_{\text{eff}} \lesssim 0.28$ [104] could be improved by 1 or 2 orders of magnitude with future CMB experiments such as [105–108].

2.4 PBH formation from strong first-order phase transition

A first order phase transition can lead to formation of black holes [68, 73, 79, 80] in different ways. In particular, due to the stochastic nature of nucleation, there is a probability that some regions remain for a longer time in the false vacuum while the space around them gets filled by true vacuum. Re-heating in the true vacuum leads to radiation, so that its energy density ρ_{true} dilutes, while the energy density in the false vacuum is $\rho_{\text{false}} \simeq V_{\Lambda}$. Thus regions in the false vacuum become relatively denser as quantified by $\delta \equiv \rho_{\text{false}}/\rho_{\text{true}} - 1$. If a region in the false vacuum (approximated as roughly-spherical) has radius larger than roughly the Hubble parameter, it forms a primordial black hole when the density contrast exceeds the critical value $\delta_c \approx 0.45$ [109].

According to [80] the resulting probability that a Hubble patch forms a PBH in a supercooled first-order phase transition, with $\alpha \gtrsim 100$ and inverse duration $\beta/H \lesssim 10$, is analytically approximated by

$$\mathcal{P}_{\text{coll}} \approx \exp \left[-a \left(\frac{\beta}{H} \right)^b (1 + \delta_c)^{c\beta/H} \right]. \quad (2.25)$$

where $a = 0.5646$, $b = 1.266$ and $c = 0.6639$. The collapse probability does not depend on α in the limit of strong supercooling $\alpha \gg 1$ where the residual initial radiation energy is negligible. The collapse probability crucially depends on the duration of the phase transition β/H , as a small enough β/H (i.e. a long enough duration) allows Hubble-sized late-blooming regions. The resulting fraction of the density of PBH with respect to the density of dark matter is

$$f_{\text{PBH}} \equiv \frac{\rho_{\text{PBH}}}{\rho_{\text{DM}}} \approx \frac{\mathcal{P}_{\text{coll}}}{2.2 \times 10^{-11}} \frac{T_{\text{eq}}}{140 \text{ GeV}}. \quad (2.26)$$

where $\mathcal{P}_{\text{coll}}$ is given in eq. (2.25), and T_{eq} is the temperature at which vacuum and radiation have the same density, eq. (2.4). So $f_{\text{PBH}} \sim 1$ roughly corresponds to $\beta/H \sim 8$. This value is realized when the couplings of the model are mildly small and the tunnelling is near to being too slow for the phase transition to complete, such that the nucleation temperature is low.

PBH can explain all DM, $f_{\text{PBH}} = 1$, in the mass range (see [110] for a review)

$$10^{-16} M_{\odot} \lesssim M_{\text{PBH}} \lesssim 3 \times 10^{-12} M_{\odot}. \quad (2.27)$$

PBH form with mass roughly given by the mass within the sound horizon volume at bubble collision time,

$$M_{\text{PBH}} \approx k \frac{4\pi}{3} \left(\frac{c_s}{H}\right)^3 \rho_{\text{rad}}^{\text{late}} \Big|_{t_{\text{coll}}} \approx M_{\odot} \left(\frac{20}{g_{\star}(T_{\text{eq}})}\right)^{1/2} \left(\frac{0.14 \text{ GeV}}{T_{\text{eq}}}\right)^2 \quad (2.28)$$

where $g_{\star} \approx 100$, $M_{\odot} \approx 2 \times 10^{30} \text{ kg}$ is the solar mass, $c_s \simeq 1/\sqrt{3}$ is the sound speed, $k \lesssim 1$, $\rho_{\text{rad}}^{\text{late}}$ is the false vacuum energy in a late-patch [80]. The DM range in eq. (2.27) roughly corresponds to equilibrium temperatures $50 \text{ TeV} \lesssim T_{\text{eq}} \lesssim 10 \text{ PeV}$.

Spin of the primordial black holes

It is interesting to assess the small initial spin of the PBH since mechanisms for its growth have been explored [111–113]. The spin of the PBH is parameterized by the dimensionless Kerr parameter a_* , with variance approximated by [84, 86, 114–116]

$$\langle a_*^2 \rangle^{1/2} \simeq \frac{4.0 \cdot 10^{-3} \sqrt{1 - \gamma^2}}{1 + 0.036 [21 - 2 \log_{10}(f_{\text{PBH}}/10^{-7}) - \log_{10}(M_{\text{PBH}}/10^{15} \text{g})]}. \quad (2.29)$$

The parameter γ typically lies in the range $0.81 - 1$; we assume a reference value $\gamma = 0.96$ [115, 116].

3 Minimal model with singlet scalar DM

We now start to compute the signals of various models. We start from a minimal model of dynamical electroweak symmetry breaking, that involves two extra scalars s and s' besides the Standard Model Higgs doublet H . Assuming, for simplicity, that the theory is separately invariant under $s \rightarrow -s$ and $s' \rightarrow -s'$, the discrete symmetry $\mathbb{Z}_2 \otimes \mathbb{Z}'_2$ allows the scale invariant potential

$$V_{\text{tree}} = V_{\Lambda} + \lambda_H |H|^4 + \frac{\lambda_S}{4} s^4 + \frac{\lambda_{S'}}{4} s'^4 + \frac{\lambda_{HS}}{2} |H|^2 s^2 + \frac{\lambda_{HS'}}{2} |H|^2 s'^2 + \frac{\lambda_{SS'}}{4} s^2 s'^2. \quad (3.1)$$

Benchmark points	A	B	C	D
Scalon mass m_s in TeV	59.5	200	10^3	10^4
DM mass $m_{s'}$ in PeV	0.84	2.72	12.7	114
Equilibrium temperature T_{eq} in TeV	59	190	890	7996
Nucleation temperature T_{nuc} in GeV	0.3	2.7	47	2600
Percolation temperature T_{perc} in GeV	0.1	1.1	29	2580
Duration of the phase transition β/H_n	6.5	6.6	6.7	6.9
PBH mass M_{PBH}/M_\odot	$2.5 \cdot 10^{-12}$	$2.4 \cdot 10^{-13}$	$1.1 \cdot 10^{-14}$	$1.4 \cdot 10^{-16}$
PBH abundance $f_{\text{PBH}} = \rho_{\text{PBH}}/\rho_{\text{DM}}$	≈ 1	≈ 1	≈ 1	≈ 1
Tuning $\Delta = d \ln f_{\text{PBH}}/d \ln m_{s,(s')}$	935 (970)	966 (1004)	1008 (1052)	1061 (1115)
PBH spin $\langle a_*^2 \rangle^{1/2}$	0.00111	0.00107	0.00102	0.00096
GW abundance $\Omega_{\text{col}}^{\text{peak}} h^2$	$1.31 \cdot 10^{-8}$	$1.29 \cdot 10^{-8}$	$1.24 \cdot 10^{-8}$	$1.19 \cdot 10^{-8}$
GW frequency $f_{\text{col}}^{\text{peak}}$ in Hz	$7 \cdot 10^{-8}$	$6.3 \cdot 10^{-7}$	$1.1 \cdot 10^{-5}$	$6.3 \cdot 10^{-4}$

Table 1. Benchmark points. The first two rows, together with $\ln R = -10$, define the parameter values. The other rows show the resulting predictions. Fig. 1 illustrates the associated gravitational waves, and fig. 2 illustrates the associated PBH mass and abundance.

A constant term V_Λ is added such that $V = 0$ at its minimum. Effects due to the explicit breaking of the scale symmetry are Planck-suppressed. The scalar s' has been introduced such that the couplings λ_S and λ_{HS} run with β functions

$$\beta_{\lambda_S} \simeq \frac{\lambda_{SS'}^2}{2(4\pi)^2}, \quad \beta_{\lambda_{HS}} \simeq \frac{\lambda_{SS'}\lambda_{HS'}}{(4\pi)^2} \quad (3.2)$$

that can make them negative at lower energy, inducing dynamical symmetry breaking. This theory admits multiple symmetry-breaking patterns depending on which combination of couplings crosses zero first. Following [117] we define a parameter R that controls which effective running coupling turns negative first:

$$\lambda_S^{\text{eff}}(s) = \frac{\beta_{\lambda_S}}{2} \ln \frac{s^2}{e^{1/2} w^2}, \quad \lambda_{HS}^{\text{eff}}(s) = \frac{\beta_{\lambda_{HS}}}{2} \ln \frac{R s^2}{w^2}. \quad (3.3)$$

We are interested in the phase where s and h acquire vacuum expectation values, $\langle s \rangle = w \gg \langle h \rangle = v = 246.2$ GeV. This phase happens for $R \lesssim 1$ when couplings cross the critical boundary $\lambda_{HS} = -2\sqrt{\lambda_H \lambda_S}$ while λ_{HS} is negative. The standard Gildener-Weinberg approximation applies at $R \ll 1$, such that λ_{HS} has a roughly constant value. Phenomenology remains viable when R is mildly smaller than 1 and multi-phase effects (encoded in the running of λ_{HS}) become relevant [117, 118].

As the Higgs mass is known to be $m_h \approx 125.1$ GeV, we use as free parameters the masses of s and s' and R . The various couplings are then approximated in terms of our parameters as [117]

$$\lambda_{SS'} \approx \frac{(4\pi)^2 m_s^2}{m_{s'}^2}, \quad \lambda_{HS'} \approx -\frac{(4\pi)^2 m_h^2}{m_s^2 \ln R}, \quad w \simeq \frac{\sqrt{2} m_{s'}}{4\pi m_s}. \quad (3.4)$$

Furthermore, s' is a stable DM candidate in the phase with $\langle s' \rangle = 0$. The s' relic abundance can match the DM abundance in two different ways: at moderately large coupling via freeze-out at $T_{\text{dec}} \approx m_{s'}/25$; at small coupling via super-cooling [119]. We focus on the first regime.

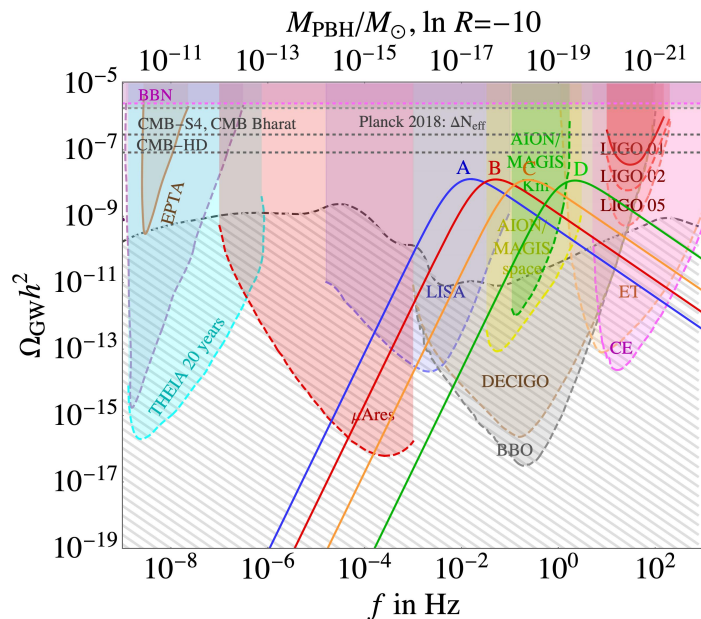


Figure 1. Gravitational wave spectrum as a function of frequency f at the benchmark points A, B, C, D listed in table 1. The predicted gravitational wave signals (colored curves) fall within the sensitivity curves of possible future gravitational wave detectors (dashed shaded regions). The upper axis shows the mass of the corresponding primordial black holes. The gray hatched curve shows the expected astrophysical foreground.

The re-heating temperature T_{RH} of eq. (2.5) is $T_{\text{RH}} \approx 0.07 m_{s'}$, a factor of 2 larger than T_{dec} . So this freeze-out regime is realized. The s -wave DM annihilation cross section σ_0 and the spin-independent direct detection cross section are [117]

$$\sigma_0 \simeq \frac{\lambda_{SS'}^2 + 4\lambda_{HS'}^2}{64\pi m_{s'}^2}, \quad \sigma_{\text{SI}} \simeq \frac{64\pi^3 f_N^2 m_N^4}{m_{s'}^6} \quad (3.5)$$

with $f_N \approx 0.3$ and $m_N \approx 0.946 \text{ GeV}$. The cosmological DM abundance is reproduced when $\sigma_0 \approx 1/M^2$ with $M \approx 23 \text{ TeV}$. Current bounds on direct detection are satisfied for $m_{s'} \gtrsim 2 \text{ TeV}$ [117, 120].

As PBH provide a second DM candidate, we will also consider the possibility that s' is unstable, such that s' no longer is DM, and acquires more visible collider signals. Destabilization of s' happens if the \mathbb{Z}_2 symmetry is broken either spontaneously by $\lambda_{SS'} < 0$, or explicitly. For example, s or s' might linearly couple to right-handed neutrinos allowing to generate neutrino masses [121].

The thermal potential is approximated by eq. (2.11) with

$$m^2 = \left(\frac{\lambda_{SS'}}{2} + 2\lambda_{HS} \right) \frac{T^2}{12}, \quad k = \frac{\lambda_{SS'}^{3/2} + 4\lambda_{HS}^{3/2}}{2\sqrt{2}} \frac{T}{4\pi}, \quad \lambda = \beta_{\lambda_S} \ln \frac{w}{T} \quad (3.6)$$

The phase transition is ended by nucleation if $S_3/T \sim 16\sqrt{6}\pi^3 \lambda_{SS'}^{-3/2} / \ln(w/T) > 4 \ln M_{\text{Pl}}/T$, implying a not too small coupling $\lambda_{SS'}$ [122]. While this rough estimate qualitatively explains the main results, gravitational wave and primordial black holes are more precisely computed numerically.

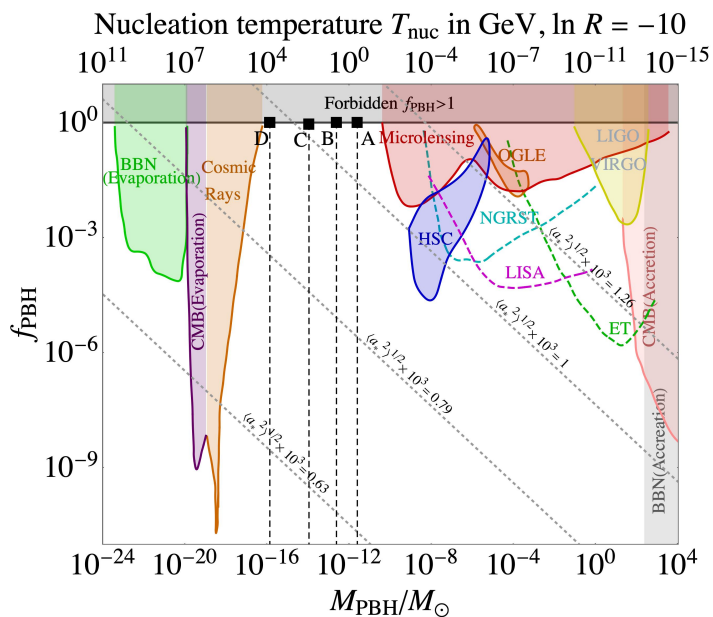


Figure 2. Prediction of the A, B, C, D benchmark points of table 1 for the primordial black holes mass and for their cosmological abundance f_{PBH} in units of the DM abundance. The colored regions with solid borders are excluded. Dashed curves indicate future experimental sensitivities. Diagonal dotted lines represent different values of PBH spin.

3.1 Primordial Black Holes as DM

We start the analysis by focusing in table 1 on some benchmark point in parameter space, all with $\ln R = -10$, and with $m_s, m_{s'}$ selected such that nucleation happens after a significant amount of super-cooling. Then, all points predict significant comparable amount of GW, $\Omega_{\text{GW}} \sim 10^{-8}$. As shown in fig. 1 the GW frequency spectra mostly differ by position of the peak, given by eq. (2.22). The peak frequency is lower at larger values of $m_{s,s'} \gg v$, which remains compatible with generating the weak scale v thanks to small enough values of λ_{HS} . Fig. 1 also shows the expected sensitivity reaches of possible future GW observatories, broadly classified as:

- Ground-based interferometer detectors at higher f : aLIGO/aVIRGO (red dashed) [31, 32, 123], AION [12] (orange solid), EINSTEIN TELESCOPE (ET) [20, 124] (blue solid), COSMIC EXPLORER (CE) [21, 125] (blue dashed). LIGO-VIRGO provide the only existing bound [8]. We also show the projected sensitivity at the end of the next advanced LIGO-VIRGO phase [31, 32, 123].
- Space-based interferometers: LISA [15, 126] (pink solid), BBO [19, 127] (green dashed), DECIGO/U-DECIGO [18, 128] (green solid), AEDGE [13, 129] (orange dashed), μ -ARES [14] (magenta dashed). These probe the mHz frequency range in which PBH from a supercooled FOPT can explain all the DM abundance.
- Lower frequencies are probed by recast of astrometry proposals GAIA/THEIA [10] (brown dashed), and by pulsar timing arrays: SKA [9] (purple), EPTA [130, 131] (purple dashed), NANOGRAV [2] (blue shaded region).

The GW signals are above the expected astrophysical backgrounds, shown by the hatched curve in fig. 1 (see [132] for a list of references).

Next, fig. 2 illustrates the predicted mass of abundance of Primordial Black Holes at the benchmark points. We choose points within the mass range where PBH can be all of DM, and fixed the parameters $m_{s,s'}$ such that PBH match the cosmological DM abundance, $f_{\text{PBH}} = 1$. In this region the PBH abundance has a strong sensitivity to model parameters,

$$\Delta \equiv \frac{\partial \ln f_{\text{PBH}}}{\partial \ln m_{s,s'}} \sim 1000. \quad (3.7)$$

Table 1 shows precise sensitivity values at the benchmark points. A similar sensitivity arises in theories where PBH are produced via enhanced primordial inhomogeneities (although specific models can be more tuned).

Fig. 2 also depicts existing constraints on f_{PBH} (see [133–136] for details on constraints):

- Hawking evaporation of PBH is relevant at lower M_{PBH} and implies constraints using data from CMB [137], EDGES [138], INTEGRAL [139, 140], VOYAGER [141], 511 keV [142], EGRB [143].
- Micro-lensing observations from HSC [144], EROS [145], ICARUS [146], including a PBH hint of PBH from OGLE [147]. The dashed curve shows the micro-lensing future sensitivity of the NGRST [148].
- The range $M_{\text{PBH}} \sim M_{\odot}$ is constrained by LIGO-VIRGO-KAGRA (LVK) observations of PBH-PBH mergers [149–155]. Future GW interferometers like ET and LISA are expected to reach the sensitivities depicted as dashed curves [156–161]. PBH are expected to accrete leading to extra constraints adopted from [162, 163].

3.2 General parameter space of the model

We next move from the benchmark points to explore the full parameter space of the model. We show plots as function of the DM mass $m_{s'}$ and of the dilaton mass m_s at fixed values of $\ln R$, focusing on two values:

- $\ln R = -10$, in the Gildner-Weinberg regime;
- $\ln R = -1/2$, where λ_{HS} is as small as allowed by its running and multi-phase effects become relevant [117].

Fig. 3 shows contour levels of the nucleation temperature and of the inverse duration β/H of the phase transition. Interesting values are obtained in a region ranging from too large non-perturbative couplings down to too small couplings, where the phase transition is ended in a too rapid way by QCD rather than by nucleation [81, 164]. Fig. 4 shows, in the same plane, contour values of the PBH masses. Fig. 5 shows contour values of the PBH abundance. As it is exponentially sensitive to parameter values, the figures focuses on a small portion of the parameter space where the PBH abundance is around the DM abundance.

Next, we overlay various main results in fig. 6.

Assuming that s' is stable, we here show its relic freeze-out abundance: it matches the cosmological DM abundance along the green curve, and gets larger above the green curve. Furthermore, the PBH abundance matches the DM abundance along the red curve, and gets

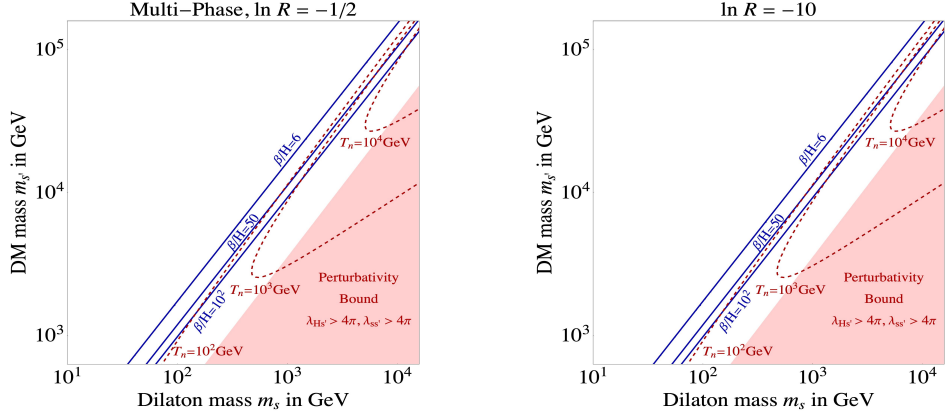


Figure 3. Contour levels of the nucleation temperature T_{nuc} (red dashed curves) and of the inverse duration of the phase transition β/H . A significant amount of PBH are produced at $\beta/H \lesssim 8$.

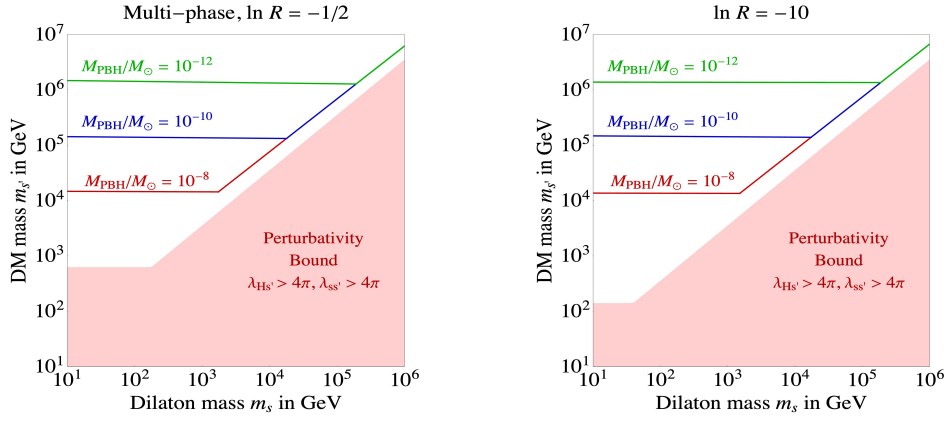


Figure 4. Contour-levels of the mass of produced primordial black holes.

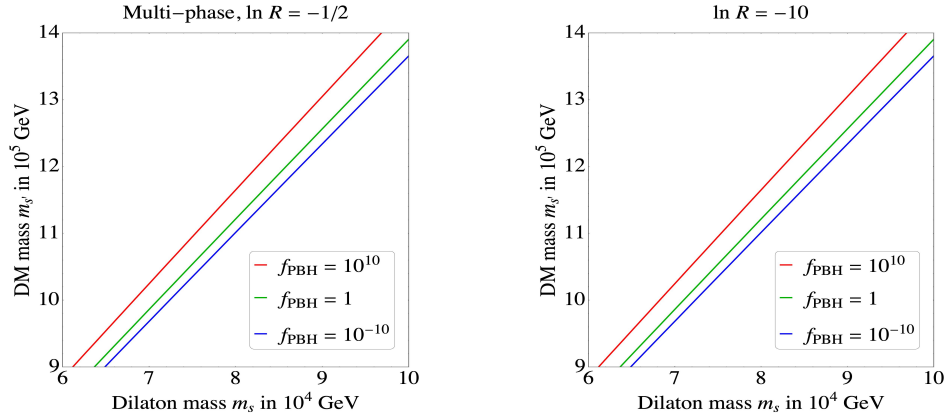


Figure 5. Contour levels of the cosmological abundance of Primordial Black Holes.

larger above. In general, the abundances of the two DM candidates (PBH and s') should be summed. The plot shows that s' particle DM dominates over PBH in most of the allowed parameter range (unshaded region in fig. 6). The portion around $m_s \sim 200 \text{ GeV}$ where $f_{\text{PBH}} \sim 1$ has $M_{\text{PBH}} \sim 10^{-5} M_\odot$, above the mass range where PBH can be all DM. Assuming instead that s' is unstable, PBH provide DM in a different portion of the parameter space, along the red curve.

Fig. 6 also shows that significant GW signals arise in the white allowed region (see also [165]). Each future GW experiment would probe the region in parameter space above the indicated curve, up to the allowed boundary where $f_{\text{PBH}} \approx 1$. We do not study the region of parameter space where QCD (rather than nucleation) ends the phase transition. More in detail, fig. 7 shows how the various possible GW experiments cover the parameter space, by being sensitive to different frequencies. As a specific example, fig. 8 shows that the expected Signal-to-Noise Ratio at LISA can reach large values. However, we here neglected the astrophysical foregrounds, expected with the spectrum illustrated in fig. 1. It's difficult to anticipate how much foregrounds will limit the sensitivity to primordial GW, as some foregrounds can be partially subtracted.

3.3 Particles as DM

If s' is stable, in most of the parameter space the DM abundance is dominated by its relic freeze-out abundance rather than by primordial black holes. It is then interesting to explore the gravitational waves signals that arise under the assumption that thermal relic particle DM makes all the cosmological DM abundance. Since the spectrum of gravitational waves produced from bubble collisions is roughly universal, eq. (2.21), gravitational waves can be characterised by their peak frequency and abundance. Fig. 9 shows the predictions for such two quantities for different values of the DM mass (squared points).

4 Model with SU(2) vector DM

As a second model, we add to the SM a complex scalar S doublet under an extra ‘dark’ $\text{SU}(2)_X$ gauge group with gauge coupling g_X [119]. The dimension-less potential is

$$V_{\text{tree}} = V_\Lambda + \lambda_H |H|^4 + \lambda_S |S|^4 + \lambda_{HS} |HS|^2. \quad (4.1)$$

In the unitary gauge the scalars can be expanded as

$$S = \frac{1}{\sqrt{2}} \begin{pmatrix} 0 \\ s \end{pmatrix}, \quad H = \frac{1}{\sqrt{2}} \begin{pmatrix} 0 \\ h \end{pmatrix}. \quad (4.2)$$

The relevant one-loop β functions is

$$\beta_{\lambda_S} \simeq \frac{1}{(4\pi)^2} \frac{9g_X^4}{8} \quad (4.3)$$

while, in this model, λ_{HS} only gets multiplicatively renormalized, and can be approximated as constant. The $\text{SU}(2)_X$ vectors acquire a mass $M_X = g_X w/2$ and are stable DM candidates [166]. Like in the previous model, we again use as free parameters the dilaton mass m_s and the DM mass M_X . The other couplings are then approximated in terms of them as [117]

$$g_X \simeq \frac{4\pi\sqrt{2}m_s}{3M_X}, \quad \lambda_{HS} \simeq -\frac{8\pi^2 m_h^2 m_s^2}{9M_X^4}, \quad w \simeq \frac{3M_X^2}{2\sqrt{2}\pi m_s}. \quad (4.4)$$

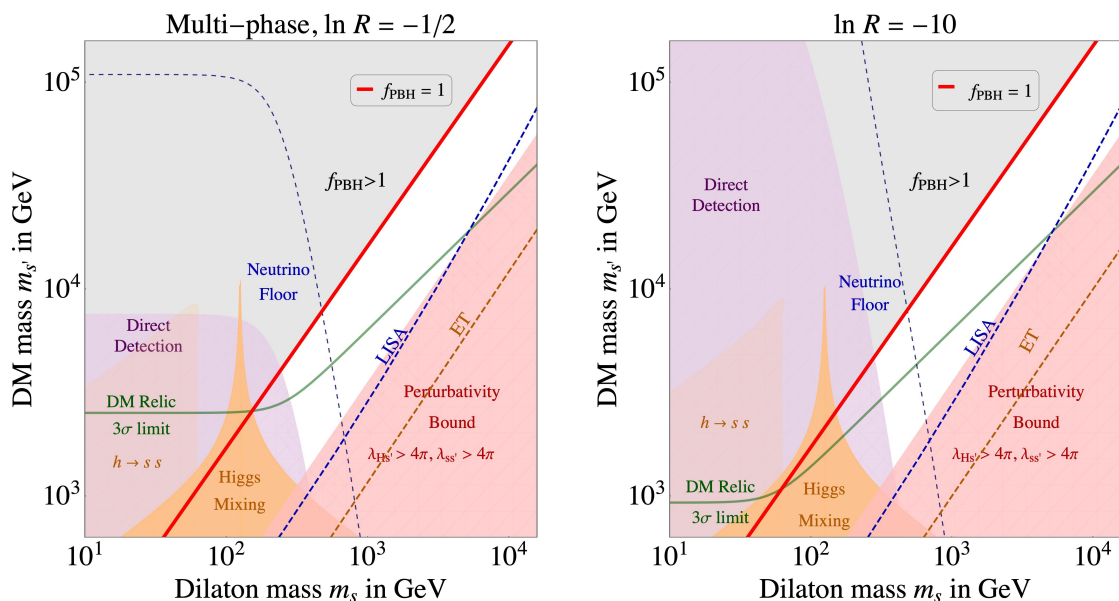


Figure 6. Summary plot for the minimal model. The right panel assumes a larger mixed quartic λ_{HS} , while in the left panel λ_{HS} is so small that its running leads to multi-phase effects. The cosmological relic abundance of particle (of Primordial Black Hole) DM is over-abundant above the green (red) curve. Gravitational waves appear detectable above the curves indicated as LISA and ET. The shaded regions are excluded by DM direct detection (purple); Higgs $h \rightarrow ss$ decays (beige); bounds on Higgs/dilaton mixing (orange); too large quartic couplings (pink).

The mixing angle between the Higgs and the scalaron is

$$\sin 2\theta = \frac{v^2 \sqrt{8\lambda_H |\lambda_{HS}|}}{m_s^2 - m_h^2}. \quad (4.5)$$

The s -wave cross-sections for DM annihilations $XX \leftrightarrow ss$ plus semi-annihilations $XX \leftrightarrow Xs$ and for DM direct detection are [166]

$$\sigma_0 = \frac{65g_X^4}{6912\pi M_X^2} = \frac{260\pi^3 m_s^4}{2187M_X^8}, \quad \sigma_{\text{SI}} \simeq \frac{64\pi^3 f_N^2 m_N^4}{81M_X^6}. \quad (4.6)$$

The cosmological DM abundance is again reproduced when $\sigma_0 \approx 1/(23 \text{ TeV})^2$. We restrict our analysis to the regime where $g_X \sim 1$ is large enough that super-cooling is ended by nucleation, rather than by QCD. Then $T_{\text{RH}} = (136/64g_*)^{1/4} M_X/\pi \approx M_X/8.5$ is again larger than the DM decoupling temperature.

The above discussion shows that, up to order unity factors, the physics is qualitatively similar to the minimal singlet model of section 3. So the analysis proceeds in parallel: the main results are summarised by the left panel of fig. 10, which is similar to fig. 6 for the minimal singlet model. Predictions for gravitational waves under the assumption that particle DM matches the cosmological DM density [45, 166] are shown in fig. 9 (circle points). The squared points show the predictions of the minimal s' model discussed in the previous section.

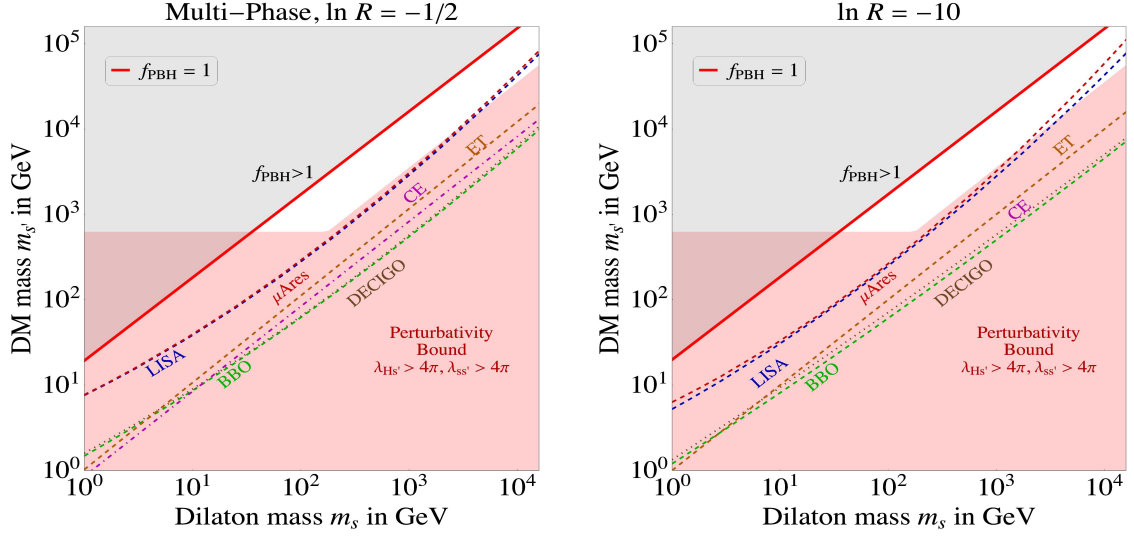


Figure 7. GW are observable inside the bands. Only zoomed in for LISA and CE GW detectors on the left and showing all GW detectors on the right. The arrows show the range of the parameter space that will see a signal in LISA after 4 years of running.

The predictions of the two models are qualitatively similar, up to order unity factors, because different models share the following common feature: DM induces the running and the thermal potential for dynamical symmetry breaking.

The phase transition in the non-scale-invariant version of the model was studied in [167].

5 Model with $U(1)_{B-L}$ gauge group

Finally, we consider a similar model where the dark gauge group is now an Abelian $U(1)$ factor. Unlike in the $SU(2)$ model, the $U(1)$ vector is not a stable DM candidate, as long as no extra symmetry is added to forbid its kinetic mixing with the hyper-charge $U(1)_Y$ vector. Furthermore, the extra $U(1)$ needs not to be dark, as the SM field content allows for a possible $U(1)_{B-L}$ extra gauge symmetry. We identify $U(1)$ with $U(1)_{B-L}$ and denote as g_{B-L} its gauge coupling, and as Z' its vector. To break $U(1)_{B-L}$, the scalar S must have a non-vanishing charge q_S under $U(1)_{B-L}$. The case $q_S = 2$ is often considered, such that S can also provide mass to the right-handed neutrinos via a Yukawa coupling. The following considerations largely depend only on the product $q_S g_{B-L}$. The scalar potential is

$$V_{\text{tree}} = V_\Lambda + \lambda_H |H|^4 + \lambda_S |S|^4 + \lambda_{HS} |HS|^2. \quad (5.1)$$

In the unitary gauge the scalars can be expanded as

$$S = \frac{s}{\sqrt{2}}, \quad H = \frac{1}{\sqrt{2}} \begin{pmatrix} 0 \\ h \end{pmatrix}. \quad (5.2)$$

At one loop, the λ_S quartic runs as

$$\beta_{\lambda_S} \simeq \frac{6(q_S g_{B-L})^4}{(4\pi)^2}. \quad (5.3)$$

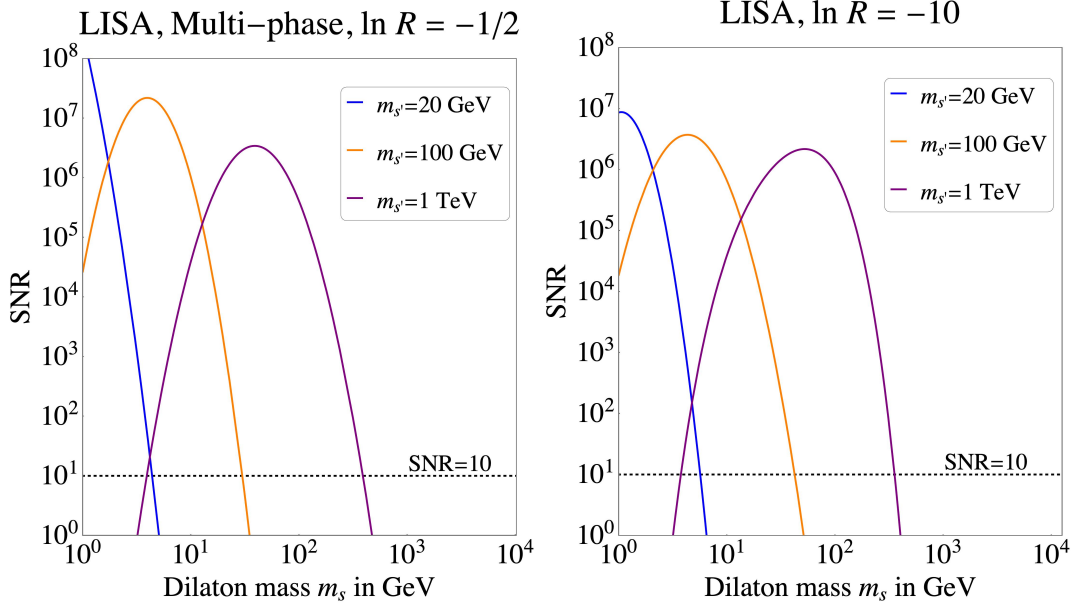


Figure 8. *Expected Signal-Noise Ratio. at LISA as function of the dilaton m_s for different fixed values of the DM mass $m_{s'}$, and neglecting astrophysical foregrounds. A $\text{SNR} \gtrsim 10$ allows GW detection.*

We use as free parameters m_s and $M_{Z'}$, in order to proceed in parallel with the previous models (although Z' is now not a DM candidate). The other parameters are then approximated in terms of m_s and $M_{Z'}$ as

$$q_S g_{B-L} \simeq \sqrt{\frac{2}{3}} \frac{2\pi m_s}{M_{Z'}}, \quad \lambda_{HS} \simeq -\frac{8\pi^2 m_h^2 m_s^2}{3M_{Z'}^4}, \quad w \simeq \sqrt{\frac{3}{2}} \frac{M_{Z'}^2}{2\pi m_s}. \quad (5.4)$$

At the minimum $\langle s \rangle = w$ the $U(1)_{B-L}$ Z' vector acquires mass $M_{Z'} = q_S g_{B-L} w$ and decays quickly. In this model no particle DM candidate is present, and only primordial black holes can provide DM. Furthermore, electroweak precision data imply $M_{Z'}/g_{B-L} \gtrsim 7 \text{ TeV}$ [168, 169] up to corrections due to kinetic mixing with hypercharge. The re-heating temperature is $T_{\text{RH}} = T_{\text{infl}} = M_{Z'}(45/64\pi^4 g_*)^{1/4} \approx M_{Z'}/11$. The s thermal potential is $V_T \approx 3T^4 J_B(q_S^2 g_{B-L}^2 s^2/T^2)/2\pi^2$, leading in eq. (2.11) to the thermal mass $m = q_S g_{B-L} T/2$, and to the cubic $k = 3(q_S g_{B-L})^3 T/4\pi$. The right-handed panel of fig. 10 summarises our results for this model. PBH have the DM abundance along the red curve, and their mass falls in the region where PBH can be DM in the green region. This is compatible with $T_{\text{nuc}} \gtrsim \text{GeV}$, such that super-cooling is ended by nucleation. Again, gravitational waves arise at a detectable $\Omega_{\text{GW}} \sim 10^{-8}$ level. Such conclusions agree with a previous study [81].

6 Discussion and Conclusion

We investigated various models of dynamical breaking of the electroweak symmetry. A common feature is that an extra scalar s , neutral under the SM gauge group, is added to the Higgs sector. Some extra particle is needed to mediate quantum corrections to the s potential such that s acquires a vacuum expectation value. Different models introduce different particles: the minimal model employs one extra scalar s' ; other models employ vectors of an extended $U(1)$ or $SU(2)$ gauge group.

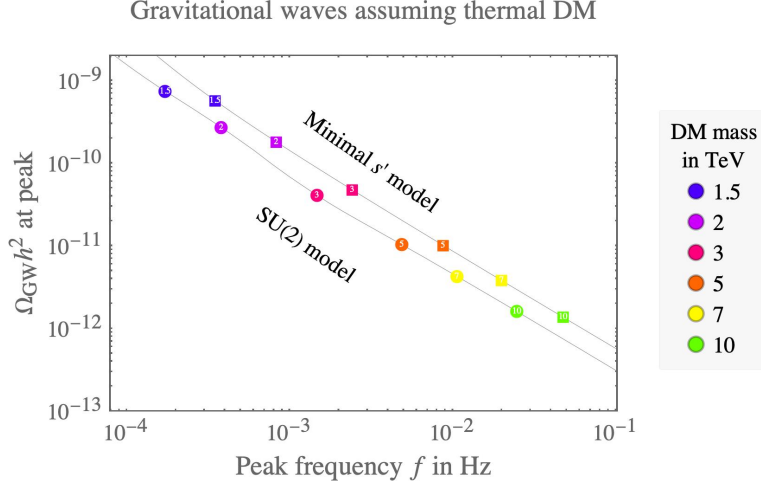


Figure 9. Predicted peak frequency and abundance of gravitational waves as function of the particle DM mass, assuming that it reproduces the cosmological DM abundance, in the two models of section 3 and 4.

In all cases the cosmological phase transition is strongly first order, leading to Gravitational Waves (at a level detectable by realistic future observatories) and to Primordial Black Holes (at a level that, in a part of the parameter space, can account for the Dark Matter relic density of the universe). The PBH mass depends on the parameters of the model and can fall in the range where PBH can be all of DM; this parameter space can be tested by GW signals.

In the minimal model, this is illustrated by the examples in fig. 2. Fig. 1 shows that such a range leads to detectable GW with μHz -mHz frequencies, while the new s and s' particles are too heavy to give signals at current particle colliders. The model already contains one possible DM candidate, as the scalar s' can be stable. In this case, the s' thermal freeze-out relic abundance dominates over the black hole abundance. The regime of particle DM is realized when particles have lighter TeV-scale mass, leading to collider signals mostly from s /Higgs mixing, direct detection signals, and GW with lower frequency in the μHz -nHz range.

A similar situation is encountered in the SU(2) model, where the SU(2) vectors are stable DM candidates.

The vector present in the U(1) model can instead decay via a kinetic mixing with hyper-charge and/or because SM fermions are charged under it (the U(1) can be identified as $U(1)_{B-L}$). Primordial black holes can have appropriate mass and abundance to explain Dark Matter.

Primordial black holes and gravitational waves in the same frequency range can also be generated by different theories, where inflation produces large curvature perturbations at small scales, see e.g. [170]. The GW spectral shapes arising from second-order tensor perturbations are different from those produced due to bubble collisions during phase transitions.

Acknowledgement

We thank Luca Marzola for collaboration and discussion during the initial stage of the project, Marcos Flores and Tomer Volansky for discussions.

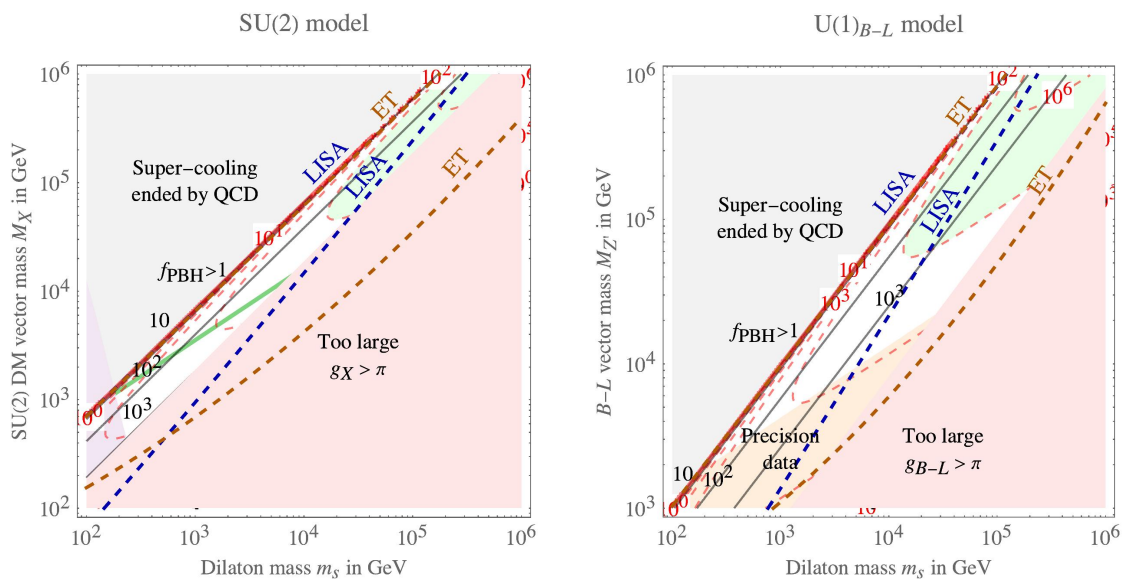


Figure 10. Summary plots for the models based on an extra dark SU(2) (left) or U(1)_{B-L} model (right). The curves mostly have the same color coding as in the summary plot for the minimal model, fig. 6. The cosmological relic abundance of particle (of Primordial Black Hole) DM is over-abundant above the green (red) curve. The shaded regions are excluded by DM direct detection (purple); bounds on precision data (orange); too large quartic couplings (pink). We omit the sub-leading bounds from $h \rightarrow ss$ and h/s mixing. We also show contour curves of T_{nuc} (red dashed) and of β/H (black solid). Stochastic gravitational waves are observed in the regions inside the dashed curves, at the indicated possible future detectors.

References

- [1] LIGO and VIRGO Collaborations, Phys. Rev. Lett. 116 (2016) 061102 [arXiv:1602.03837].
- [2] NANOGrav collaboration, Astrophys. J. Lett. 951 (2023) L8 [arXiv:2306.16213].
- [3] EPTA, INPTA collaborations, Astron. Astrophys. 678 (2023) A50 [arXiv:2306.16214].
- [4] PPTA collaboration, Astrophys. J. Lett. 951 (2023) L6 [arXiv:2306.16215].
- [5] CPTA collaboration, Res. Astron. Astrophys. 23 (2023) 075024 [arXiv:2306.16216].
- [6] LIGO and VIRGO Collaborations, Phys. Rev. Lett. 118 (2017) 121101 [arXiv:1612.02029].
- [7] LIGO and VIRGO Collaborations, Phys. Rev. D 100 (2019) 061101 [arXiv:1903.02886].
- [8] KAGRA, VIRGO, LIGO Collaborations, Phys. Rev. D 104 (2021) 022004 [arXiv:2101.12130].
- [9] SKA Collaboration, Publ. Astron. Soc. Austral. 37 (2020) e002 [arXiv:1810.02680].
- [10] J. Garcia-Bellido, H. Murayama, G. White, JCAP 12 (2021) 023 [arXiv:2104.04778].
- [11] S. Baum, Z. Bogorad, P.W. Graham, JCAP 05 (2024) 027 [arXiv:2309.07952].
- [12] AION Collaboration, JCAP 05 (2020) 011 [arXiv:1911.11755].
- [13] AEDGE Collaboration, EPJ Quant. Technol. 7 (2020) 6 [arXiv:1908.00802].
- [14] A. Sesana et al., Exper. Astron. 51 (2021) 1333 [arXiv:1908.11391].
- [15] LISA Collaboration, arXiv:1702.00786.
- [16] TIANQIN Collaboration, Class. Quant. Grav. 33 (2016) 035010 [arXiv:1512.02076].
- [17] W.H. Ruan, Z.-K. Guo, R.G. Cai, Y.-Z. Zhang, Int. J. Mod. Phys. A 35 (2020) 2050075 [arXiv:1807.09495].
- [18] DECIGO Collaboration, PTEP 2021 (2021) 05A105 [arXiv:2006.13545].

- [19] V. Corbin, N.J. Cornish, *Class.Quant.Grav.* 23 (2006) 2435 [[arXiv:gr-qc/0512039](#)].
- [20] EINSTEIN collaboration, *Class.Quant.Grav.* 27 (2010) 194002.
- [21] D. Reitze et al., *Bull.Am.Astron.Soc.* 51 (2019) 035 [[arXiv:1907.04833](#)].
- [22] N. Aggarwal et al., *Living Rev.Rel.* 24 (2021) 4 [[arXiv:2011.12414](#)].
- [23] A. Berlin et al., *Phys. Rev. D* 105 (2022) 116011 [[arXiv:2112.11465](#)].
- [24] N. Herman, L. Lehoucq, A. Füzfa, *Phys. Rev. D* 108 (2023) 124009 [[arXiv:2203.15668](#)].
- [25] T. Bringmann, V. Domcke, E. Fuchs, J. Kopp, *Phys. Rev. D* 108 (2023) L061303 [[arXiv:2304.10579](#)].
- [26] R. Roshan, G. White, [arXiv:2401.04388](#).
- [27] eLISA collaboration, *JCAP* 04 (2016) 001 [[arXiv:1512.06239](#)].
- [28] K. Kajantie, M. Laine, K. Rummukainen, M.E. Shaposhnikov, *Phys.Rev.Lett.* 77 (1996) 2887 [[arXiv:hep-ph/9605288](#)].
- [29] T. Bhattacharya et al., *Phys.Rev.Lett.* 113 (2014) 082001 [[arXiv:1402.5175](#)].
- [30] C. Grojean, G. Servant, *Phys. Rev. D* 75 (2007) 043507 [[arXiv:hep-ph/0607107](#)].
- [31] LIGO Collaboration, *Class. Quant. Grav.* 32 (2015) 074001 [[arXiv:1411.4547](#)].
- [32] VIRGO Collaboration, *Class.Quant.Grav.* 32 (2015) 024001 [[arXiv:1408.3978](#)].
- [33] P.S.B. Dev, A. Mazumdar, *Phys. Rev. D* 93 (2016) 104001 [[arXiv:1602.04203](#)].
- [34] K.A. Meissner, H. Nicolai, *Phys. Lett. B* 648 (2007) 312 [[arXiv:hep-th/0612165](#)].
- [35] S.R. Coleman, E.J. Weinberg, *Phys. Rev. D* 7 (1973) 1888.
- [36] E. Witten, *Nucl.Phys.B* 177 (1981) 477.
- [37] L. Delle Rose, G. Panico, M. Redi, A. Tesi, *JHEP* 04 (2020) 025 [[arXiv:1912.06139](#)].
- [38] B. Von Harling, A. Pomarol, O. Pujolàs, F. Rompineve, *JHEP* 04 (2020) 195 [[arXiv:1912.07587](#)].
- [39] A. Ghoshal, A. Salvio, *JHEP* 12 (2020) 049 [[arXiv:2007.00005](#)].
- [40] J. Jaeckel, V.V. Khoze, M. Spannowsky, *Phys. Rev. D* 94 (2016) 103519 [[arXiv:1602.03901](#)].
- [41] R. Jinno, M. Takimoto, *Phys. Rev. D* 95 (2017) 015020 [[arXiv:1604.05035](#)].
- [42] L. Marzola, A. Racioppi, V. Vaskonen, *Eur. Phys.J. C* 77 (2017) 484 [[arXiv:1704.01034](#)].
- [43] S. Iso, P.D. Serpico, K. Shimada, *Phys. Rev. Lett.* 119 (2017) 141301 [[arXiv:1704.04955](#)].
- [44] W. Chao, W.-F. Cui, H.-K. Guo, J. Shu, *Chin.Phys.C* 44 (2020) 123102 [[arXiv:1707.09759](#)].
- [45] I. Baldes, C. Garcia-Cely, *JHEP* 05 (2019) 190 [[arXiv:1809.01198](#)].
- [46] T. Prokopec, J. Rezaeck, B. Swiezewska, *JCAP* 02 (2019) 009 [[arXiv:1809.11129](#)].
- [47] V. Brdar, A.J. Helmboldt, J. Kubo, *JCAP* 02 (2019) 021 [[arXiv:1810.12306](#)].
- [48] C. Marzo, L. Marzola, V. Vaskonen, *Eur. Phys.J. C* 79 (2019) 601 [[arXiv:1811.11169](#)].
- [49] T. Hasegawa, N. Okada, O. Seto, *Phys. Rev. D* 99 (2019) 095039 [[arXiv:1904.03020](#)].
- [50] J. Ellis, M. Lewicki, V. Vaskonen, *JCAP* 11 (2020) 020 [[arXiv:2007.15586](#)].
- [51] A. Chikkaballi, K. Kowalska, E.M. Sessolo, *JHEP* 11 (2023) 224 [[arXiv:2308.06114](#)].
- [52] A. Ahriche, S. Kanemura, M. Tanaka, *JHEP* 01 (2024) 201 [[arXiv:2308.12676](#)].
- [53] P. Huang, K.-P. Xie, *JHEP* 09 (2022) 052 [[arXiv:2206.04691](#)].
- [54] A. Dasgupta, P.S.B. Dev, A. Ghoshal, A. Mazumdar, *Phys. Rev. D* 106 (2022) 075027 [[arXiv:2206.07032](#)].
- [55] D. Borah, A. Dasgupta, I. Saha, *JHEP* 11 (2022) 136 [[arXiv:2207.14226](#)].
- [56] A. Dasgupta, P.S.B. Dev, T. Han, R. Padhan, S. Wang, K. Xie, *JHEP* 12 (2023) 011 [[arXiv:2308.12804](#)].
- [57] A. Ghoshal, D. Mukherjee, M. Rinaldi, *JHEP* 05 (2023) 023 [[arXiv:2205.06475](#)].
- [58] M.Y. Khlopov, R.V. Konoplich, S.G. Rubin, A.S. Sakharov, [arXiv:hep-ph/9807343](#).
- [59] K. Sato, M. Sasaki, H. Kodama, K. Maeda, *Prog.Theor.Phys.* 65 (1981) 1443.
- [60] H. Kodama, M. Sasaki, K. Sato, K. Maeda, *Prog.Theor.Phys.* 66 (1981) 2052.
- [61] K. Maeda, K. Sato, M. Sasaki, H. Kodama, *Phys. Lett. B* 108 (1982) 98.
- [62] K. Sato, H. Kodama, M. Sasaki, K. Maeda, *Phys. Lett. B* 108 (1982) 103.
- [63] S.W. Hawking, I.G. Moss, J.M. Stewart, *Phys. Rev. D* 26 (1982) 2681.
- [64] H. Kodama, M. Sasaki, K. Sato, *Prog. Theor. Phys.* 68 (1982) 1979.
- [65] M. Lewicki, V. Vaskonen, *Phys.Dark Univ.* 30 (2020) 100672 [[arXiv:1912.00997](#)].
- [66] A. Ashoorioon, A. Rostami, J.T. Firouzjatee, *Phys. Rev. D* 103 (2021) 123512 [[arXiv:2012.02817](#)].

- [67] K. Kawana, K.-P. Xie, Phys. Lett. B 824 (2022) 136791 [arXiv:2106.00111].
- [68] J. Liu, L. Bian, R.-G. Cai, Z.-K. Guo, S.-J. Wang, Phys. Rev. D 105 (2022) L021303 [arXiv:2106.05637].
- [69] T.H. Jung, T. Okui, arXiv:2110.04271.
- [70] K. Hashino, S. Kanemura, T. Takahashi, M. Tanaka, Phys. Lett. B 838 (2023) 137688 [arXiv:2211.16225].
- [71] P. Huang, K.-P. Xie, Phys. Rev. D 105 (2022) 115033 [arXiv:2201.07243].
- [72] K. Kawana, P. Lu, K.-P. Xie, JCAP 10 (2022) 030 [arXiv:2206.09923].
- [73] K. Kawana, T.H. Kim, P. Lu, Phys. Rev. D 108 (2023) 103531 [arXiv:2212.14037].
- [74] M. Kierkla, A. Karam, B. Swiezewska, JHEP 03 (2023) 007 [arXiv:2210.07075].
- [75] M. Kierkla, B. Swiezewska, T.V.I. Tenkanen, J. van de Vis, JHEP 02 (2024) 234 [arXiv:2312.12413].
- [76] K. Hashino, S. Kanemura, T. Takahashi, Phys. Lett. B 833 (2022) 137261 [arXiv:2111.13099].
- [77] S. He, L. Li, Z. Li, S.-J. Wang, Sci.China Phys.Mech.Astron. 67 (2024) 240411 [arXiv:2210.14094].
- [78] T.C. Gehrman, B. Shams Es Haghi, K. Sinha, T. Xu, JCAP 10 (2023) 001 [arXiv:2304.09194].
- [79] M. Lewicki, P. Toczek, V. Vaskonen, JHEP 09 (2023) 092 [arXiv:2305.04924].
- [80] Y. Gouttenoire, T. Volansky, In-Spire:Gouttenoire:2023naa.
- [81] Y. Gouttenoire, Phys. Lett. B 855 (2024) 138800 [InSPIRE:Gouttenoire:2023pxh].
- [82] I. Baldes, M.O. Olea-Romacho, JHEP 01 (2024) 133 [arXiv:2307.11639].
- [83] A. Salvio, JCAP 12 (2023) 046 [arXiv:2307.04694].
- [84] I.K. Banerjee, U.K. Dey, arXiv:2311.03406.
- [85] D. Gonçalves, A. Kaladharan, Y. Wu, arXiv:2406.07622.
- [86] A. Conaci, L. Delle Rose, P.S.B. Dev, A. Ghoshal, arXiv:2401.09411.
- [87] R.-G. Cai, Y.-S. Hao, S.-J. Wang, Sci.China Phys.Mech.Astron. 67 (2024) 290411 [arXiv:2404.06506].
- [88] S.R. Coleman, Phys. Rev. D 15 (1977) 2929.
- [89] M. Sasaki, S.R. Coleman, Phys. Rev. D 16 (1977) 1762.
- [90] A.D. Linde, Nucl.Phys.B 216 (1983) 421.
- [91] E. Gildener, S. Weinberg, Phys. Rev. D 13 (1976) 3333.
- [92] A.J. Helmboldt, J. Kubo, S. van der Woude, Phys. Rev. D 100 (2019) 055025 [arXiv:1904.07891].
- [93] D. Barducci, E. Bertuzzo, M.A. Tupia, JHEP 07 (2021) 119 [arXiv:2011.05795].
- [94] J. Ellis, M. Lewicki, J.M. No, JCAP 04 (2019) 3 [InSPIRE:Ellis:2018mja].
- [95] P. Athron, C. Balázs, L. Morris, JCAP 03 (2023) 006 [arXiv:2212.07559].
- [96] C. Caprini, D.G. Figueroa, Class.Quant.Grav. 35 (2018) 163001 [arXiv:1801.04268].
- [97] C. Caprini et al., JCAP 03 (2020) 024 [arXiv:1910.13125].
- [98] D. Croon, G. White, JHEP 05 (2018) 210 [arXiv:1803.05438].
- [99] D.J. Weir, Phil.Trans.Roy.Soc.Lond.A 376 (2018) 20170126 [arXiv:1705.01783].
- [100] S.J. Huber, T. Konstandin, JCAP 09 (2008) 022 [arXiv:0806.1828].
- [101] R. Jinno, M. Takimoto, Phys. Rev. D 95 (2017) 024009 [arXiv:1605.01403].
- [102] M. Lewicki, O. Pujolàs, V. Vaskonen, Eur. Phys.J. C 81 (2021) 857 [arXiv:2106.09706].
- [103] M. Maggiore, Phys.Rept. 331 (2000) 283 [arXiv:gr-qc/9909001].
- [104] PLANCK Collaboration, Astron.Astrophys. 641 (2020) A6 [arXiv:1807.06209].
- [105] A. Paul, S. Roy, A.K. Saha, arXiv:2308.07855.
- [106] C. Antel et al., Eur. Phys.J. C 83 (2023) 1122 [arXiv:2305.01715].
- [107] N. Sehgal et al., Bull.Am.Astron.Soc. 51 (2019) [arXiv:1906.10134].
- [108] CMB-HD Collaboration, arXiv:2203.05728.
- [109] B. Carr, K. Kohri, Y. Sendouda, J. Yokoyama, Rept.Prog.Phys. 84 (2021) 116902 [arXiv:2002.12778].
- [110] M. Cirelli, A. Strumia, J. Zupan, arXiv:2406.01705.
- [111] S. Jaraba, J. Garcia-Bellido, Phys.Dark Univ. 34 (2021) 100882 [arXiv:2106.01436].
- [112] F. Hofmann, E. Barausse, L. Rezzolla, Astrophys.J.Lett. 825 (2016) L19 [arXiv:1605.01938].
- [113] M. Calzà, J. March-Russell, J.G. Rosa, arXiv:2110.13602.
- [114] C.-M. Yoo, T. Harada, J. Garriga, K. Kohri, PTEP 2018 (2018) 123E01 [arXiv:1805.03946].
- [115] V. De Luca, V. Desjacques, G. Franciolini, A. Malhotra, A. Riotto, JCAP 05 (2019) 018 [arXiv:1903.01179].

- [116] T. Harada, C.-M. Yoo, K. Kohri, Y. Koga, T. Monobe, *Astrophys.J.* 908 (2021) 140 [[arXiv:2011.00710](#)].
- [117] K. Kannike, N. Koivunen, A. Kubarski, L. Marzola, M. Raidal, A. Strumia, V. Vipp, *Phys. Lett. B* 832 (2022) 137214 [[arXiv:2204.01744](#)].
- [118] K. Kannike, L. Marzola, M. Raidal, A. Strumia, *Phys.Lett.B* 816 (2021) 136241 [[arXiv:2102.01084](#)].
- [119] T. Hambye, A. Strumia, D. Teresi, *JHEP* 08 (2018) 188 [[arXiv:1805.01473](#)].
- [120] LUX-ZEPLIN collaboration, [talk at the TeVPA conference, 2024/8/26](#).
- [121] V. Brdar, Y. Emonds, A.J. Helmboldt, M. Lindner, *Phys. Rev. D* 99 (2019) 055014 [[arXiv:1807.11490](#)].
- [122] V. Brdar, A.J. Helmboldt, M. Lindner, *JHEP* 12 (2019) 158 [[arXiv:1910.13460](#)].
- [123] LIGO, VIRGO Collaborations, *SoftwareX* 13 (2021) 100658 [[arXiv:1912.11716](#)].
- [124] S. Hild et al., *Class.Quant.Grav.* 28 (2011) 094013 [[arXiv:1012.0908](#)].
- [125] LIGO Collaboration, *Class. Quant. Grav.* 34 (2017) 044001 [[arXiv:1607.08697](#)].
- [126] LISA Collaboration, [[arXiv:1907.06482](#)].
- [127] J. Crowder, N.J. Cornish, *Phys. Rev. D* 72 (2005) 083005 [[arXiv:gr-qc/0506015](#)].
- [128] K. Yagi, N. Seto, *Phys. Rev. D* 83 (2011) 044011 [[arXiv:1101.3940](#)].
- [129] L. Badurina, O. Buchmueller, J. Ellis, M. Lewicki, C. McCabe, V. Vaskonen, *Phil.Trans.A.Math.Phys.Eng.Sci.* 380 (2021) 20210060 [[arXiv:2108.02468](#)].
- [130] EPTA Collaboration, *Mon. Not. Roy. Astron. Soc.* 453 (2015) 2576 [[arXiv:1504.03692](#)].
- [131] EPTA Collaboration, *Mon. Not. Roy. Astron. Soc.* 455 (2016) 1665 [[arXiv:1509.02165](#)].
- [132] A. Ghoshal, A. Strumia, *JCAP* 07 (2024) 011 [[arXiv:2311.16236](#)].
- [133] A.M. Green, B.J. Kavanagh, *J.Phys.G* 48 (2021) 043001 [[arXiv:2007.10722](#)].
- [134] A.K. Saha, R. Laha, *Phys. Rev. D* 105 (2022) 103026 [[arXiv:2112.10794](#)].
- [135] R. Laha, *Phys.Rev.Lett.* 123 (2019) 251101 [[arXiv:1906.09994](#)].
- [136] A. Ray, R. Laha, J.B. Muñoz, R. Caputo, *Phys. Rev. D* 104 (2021) 023516 [[arXiv:2102.06714](#)].
- [137] S. Clark, B. Dutta, Y. Gao, L.E. Strigari, S. Watson, *Phys. Rev. D* 95 (2017) 083006 [[arXiv:1612.07738](#)].
- [138] S. Mittal, A. Ray, G. Kulkarni, B. Dasgupta, *JCAP* 03 (2022) 030 [[arXiv:2107.02190](#)].
- [139] R. Laha, J.B. Muñoz, T.R. Slatyer, *Phys. Rev. D* 101 (2020) 123514 [[arXiv:2004.00627](#)].
- [140] J. Berteaud, F. Calore, J. Iguaz, P.D. Serpico, T. Siegert, *Phys. Rev. D* 106 (2022) 023030 [[arXiv:2202.07483](#)].
- [141] M. Boudaud, M. Cirelli, *Phys.Rev.Lett.* 122 (2019) 041104 [[arXiv:1807.03075](#)].
- [142] W. DeRocco, P.W. Graham, *Phys.Rev.Lett.* 123 (2019) 251102 [[arXiv:1906.07740](#)].
- [143] B.J. Carr, K. Kohri, Y. Sendouda, J. Yokoyama, *Phys. Rev. D* 81 (2010) 104019 [[arXiv:0912.5297](#)].
- [144] H. Niikura et al., *Nature Astron.* 3 (2019) 524 [[arXiv:1701.02151](#)].
- [145] EROS-2 Collaboration, *Astron.Astrophys.* 469 (2007) 387 [[arXiv:astro-ph/0607207](#)].
- [146] M. Oguri, J.M. Diego, N. Kaiser, P.L. Kelly, T. Broadhurst, *Phys. Rev. D* 97 (2018) 023518 [[arXiv:1710.00148](#)].
- [147] H. Niikura, M. Takada, S. Yokoyama, T. Sumi, S. Masaki, *Phys. Rev. D* 99 (2019) 083503 [[arXiv:1901.07120](#)].
- [148] W. DeRocco, E. Frangipane, N. Hamer, S. Profumo, N. Smyth, *Phys. Rev. D* 109 (2024) 023013 [[arXiv:2311.00751](#)].
- [149] G. Franciolini, I. Musco, P. Pani, A. Urbano, *Phys. Rev. D* 106 (2022) 123526 [[arXiv:2209.05959](#)].
- [150] B.J. Kavanagh, D. Gaggero, G. Bertone, *Phys. Rev. D* 98 (2018) 023536 [[arXiv:1805.09034](#)].
- [151] A. Hall, A.D. Gow, C.T. Byrnes, *Phys. Rev. D* 102 (2020) 123524 [[arXiv:2008.13704](#)].
- [152] K.W.K. Wong et al., *Phys. Rev. D* 103 (2021) 023026 [[arXiv:2011.01865](#)].
- [153] G. Hütsi, M. Raidal, V. Vaskonen, H. Veermäe, *JCAP* 03 (2021) 068 [[arXiv:2012.02786](#)].
- [154] V. De Luca, G. Franciolini, P. Pani, A. Riotto, *JCAP* 05 (2021) 003 [[arXiv:2102.03809](#)].
- [155] G. Franciolini et al., *Phys. Rev. D* 105 (2022) 083526 [[arXiv:2105.03349](#)].
- [156] V. De Luca, G. Franciolini, P. Pani, A. Riotto, *JCAP* 11 (2021) 039 [[arXiv:2106.13769](#)].
- [157] O. Pujolas, V. Vaskonen, H. Veermäe, *Phys. Rev. D* 104 (2021) 083521 [[arXiv:2107.03379](#)].
- [158] G. Franciolini, A. Maharana, F. Muia, *Phys. Rev. D* 106 (2022) 103520 [[arXiv:2205.02153](#)].
- [159] M. Martinelli, F. Scarcella, N.B. Hogg, B.J. Kavanagh, D. Gaggero, P. Fleury, *JCAP* 08 (2022) 006 [[arXiv:2205.02639](#)].
- [160] G. Franciolini et al., *Phys. Rev. D* 108 (2023) 043506 [[arXiv:2304.03160](#)].

- [161] M. Branchesi et al., JCAP 07 (2023) 068 [[arXiv:2303.15923](#)].
- [162] P.D. Serpico, V. Poulin, D. Inman, K. Kohri, Phys.Rev.Res. 2 (2020) 023204 [[arXiv:2002.10771](#)].
- [163] L. Piga et al., JCAP 12 (2022) 016 [[arXiv:2210.14934](#)].
- [164] W. Liu, K.-P. Xie, [arXiv:2408.03649](#).
- [165] P. Ghorbani, [arXiv:2408.16475](#).
- [166] T. Hambye, A. Strumia, Phys. Rev. D 88 (2013) 055022 [[arXiv:1306.2329](#)].
- [167] M.J. Ramsey-Musolf, V.Q. Tran, T.-C. Yuan, [arXiv:2408.05167](#).
- [168] G. Cacciapaglia, C. Csaki, G. Marandella, A. Strumia, Phys. Rev. D 74 (2006) 033011 [[arXiv:hep-ph/0604111](#)].
- [169] E. Salvioni, G. Villadoro, F. Zwirner, JHEP 11 (2009) 068 [[arXiv:0909.1320](#)].
- [170] G. Domènech, Universe 7 (2021) 398 [[arXiv:2109.01398](#)].